Extreme Mechanics Letters 9 (2016) 108–118

Contents lists available at ScienceDirect

Extreme Mechanics Letters

journal homepage: www.elsevier.com/locate/eml

Effects of oxygen on interfacial strength of incremental forming of materials by photopolymerization

Zeang Zhao [a,b], Xiaoming Mu [a], Jiangtao Wu [a], H. Jerry Qi [a,*], Daining Fang [b,c,*]

[a] The George W. Woodruff School of Mechanical Engineering, Georgia Institute of Technology, Atlanta, GA 30332, USA

[b] College of Engineering, Peking University, Beijing, 100871, PR China

[c] Institute of Advanced Structure Technology, Beijing Institute of Technology, Beijing, 100081, PR China

ARTICLE INFO

Article history:
Received 25 April 2016
Accepted 27 May 2016
Available online 1 June 2016

ABSTRACT

Photopolymerization is one of the most widely used methods for additive manufacturing and microfabrication of polymer structures. However, the mechanical properties of these materials, formed incrementally or layer-by-layer by photopolymerization, remain unclear. One critical issue is the strength of the interfaces between adjacent layers. During free radical photopolymerization, these interfaces are exposed to atmospheric oxygen, which is detrimental to the polymerization reaction due to radical inhibition. The influence of oxygen on the interfacial properties, however, is still not well understood. This paper investigates the effect of oxygen on the mechanical behavior of interfaces. In order to facilitate mechanical tests, the interfacial strength is investigated using a part-by-part method that mimics the conventional layer-by-layer photopolymerization process. The experiments found that oxygen enhances the interfacial strength by improving interfacial bridging macromolecular links. A theoretical model is developed to capture the interfacial evolution. Numerical studies further illustrate the role of several processing parameters such as curing condition and resin component.

1. Introduction

Photopolymerization is widely used in coatings, adhesives, dentistry, and microfabrication [1,2]. It is also one of the most popular methods used in polymer additive manufacturing (or 3D printing) [3], as photopolymerization can cure a resin in less than ten seconds, a layer-buildup speed that meets critical requirements of 3D printing. A typical photopolymerization resin contains monomer solutions and photoinitiators. Once irradiated by light, photoinitiators cleave into primary radicals and subsequently propagate by reacting with double bonds in monomers (see Fig. 1(a) for illustration) to form a network. During this process, oxygen reacts with primary or propagating radicals to form less active peroxyl radicals. [4]. The reaction is shown schematically in Fig. 1(b). The effects of oxygen have been investigated in, for example, the work of Decker et al. [5,6] and Bowman et al. [7,8]. In general, they are more pronounced near the surface where oxygen is abundant. As pointed out by Bowman et al. [8], oxygen inhibition is undesirable in most cases: it prevents photopolymerization in thin films and creates tacky surface layers for thick films. According to Jariwala et al. [9], oxygen inhibition may also influence the shape stability of 3D printed products. Several strategies were proposed by researchers to prevent this effect, including curing in an oxygen free environment, changing irradiation wavelength, optimizing initiator concentration and implementing different chemical modifications. Detailed discussions can be found in the review of Ligon et al. [10]. But in some conditions, oxygen inhibition can be useful. Dendukuri et al. [11] showed

* Corresponding authors.
E-mail addresses: qih@me.gatech.edu (H.J. Qi), fangdn@pku.edu.cn, fangdn@bit.edu.cn (D. Fang).

http://dx.doi.org/10.1016/j.eml.2016.05.012
2352-4316/

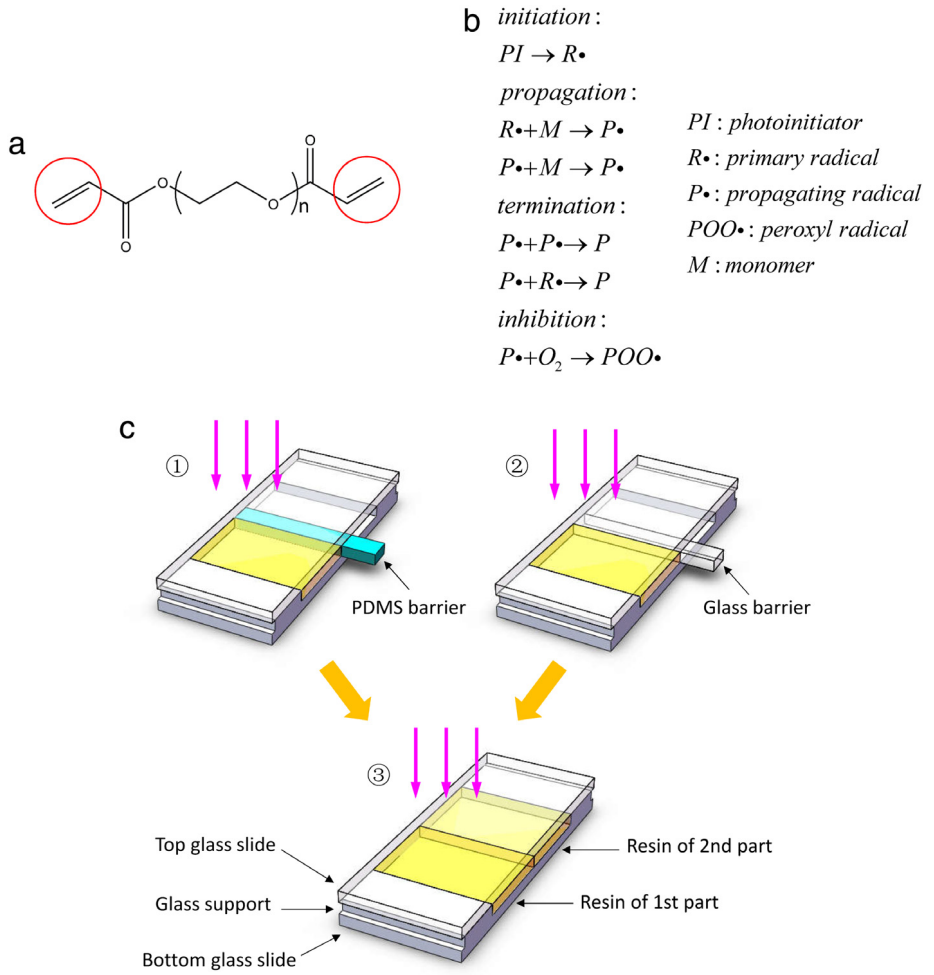

Fig. 1. Photopolymerization process. (a) Chemical structure of photo curable PEG-DA. (b) Reaction mechanism in photopolymerization. (c) Schematic graphs of sample preparations. ① Curing of the first part by inserting a PDMS barrier. ② Curing of the first part by inserting a glass barrier. ③ Curing of the whole structure after the addition of a second part.

that the tacky lubrication layer created by oxygen was essential in microfluidic fabrication of photocrosslinked particles. Jeong et al. [12] utilized oxygen-induced partial curing to fabricate hierarchical microstructures. Guvendiren et al. [13] applied the effect of oxygen in surface patterning. Our previous work [14] showed that oxygen could regulate the deformation of thin films of light active polymers. Recently, Tumbleston et al. [15] utilized the effect of oxygen to create "dead zone" interfaces in 3D printing, which accelerated the printing speed by several orders of magnitude.

The strength of the polymer interface is one of the most important concerns in applications of photopolymerization-based 3-D printing, which create structures in a layer-by-layer manner. In such applications, light irradiation is used to cure one layer of resin to a 2D pattern according to the cross-section of the 3D part. Subsequently a second layer resin is added on the top of the first and is then cured in the same manner. When this process is open to air, the chemical reactions of curing the top surface of the first layer will be inhibited by oxygen, which subsequently affects the properties of the interface between the first and the second layers. According to some researchers, for example Jeong et al. [16], the oxygen-inhibited partial curing of the surface is actually beneficial to interfacial bonding of layer-by-layer structures. A similar phenomenon is also observed in dental composites, which also involve this layer-by-layer structure. However, published studies related to dental applications mainly deal with small molecule monomers [17], which are different from those long chain crosslinkers used in 3-D printing. In addition, current results on the interfacial strength of dental composites are contradictory. Many researchers showed that oxygen inhibition is desirable to increase the interfacial strength [17–19], but some others found that oxygen seems to play no role [20]. It is apparent that many questions remain to be answered regarding the role of oxygen on interfacial strength. In addition, to our best knowledge, comprehensive studies that can provide quantitative information for 3D printing are scarce and most of them are just qualitative.

In this work, the role of oxygen on interfacial strength during incremental photopolymerization was investi-

gated. We carried out experiments on interfacial bonding under different photopolymerization processing parameters to investigate the effect of oxygen on interfacial strength. Realizing the challenge in conducting mechanical experiments on the single interface that is formed in the layer-by-layer photopolymerization method, we used an alternative approach, or the part-by-part incremental photopolymerization method. This method could facilitate mechanical characterization without significantly changing the nature of the interfaces. Based on experimental results, an interfacial model was developed to capture the evolution of interfacial strength under oxygen inhibition. Parametric studies were also conducted in order to investigate the role of oxygen for different conditions.

2. Experiments

2.1. Materials and sample preparations

The resin used in this work was a mixture of 99.28 wt% PEG-DA (Poly(ethylene glycol) (700) diacrylate; Sigma Aldrich, St. Louis, MO, USA), 0.67 wt% photoinitiator Irgacure 819 (Phenylbis (2,4,6-trimethylbenzoyl)phosphine oxide; Sigma Aldrich) and 0.05 wt% photoabsorber Sudan I (Sigma Aldrich). The phtoabsorber was added to slow down the reaction so that we could control the speed more precisely. In 3D printing, the layer-by-layer method involves hundreds to thousands of layers with a layer thickness smaller than 0.1 mm, making it a significant challenge to study individual interfaces. Here, we designed a part-by-part curing process that would maintain a similar interface but could be easily employed for mechanical tests. The fabrication process is shown schematically in Fig. 1(c). Samples were cured between two glass slides with 1 mm thick glass supports at two edges. A LED projector (D912HD, Vivitek USA, City of Industry, CA, USA) was used for irradiation perpendicular to the glass slide. At first, one half of the sample (7.5 mm × 10 mm × 1 mm) was cured for different time periods under various light intensities. Before photopolymerization of the first part, an oxygen permeable [11,16] Poly(dimethylsiloxane) (PDMS) barrier (cross section 1 mm × 0.5 mm) was inserted at the center of the glass mold to control the shape (Fig. 1(c)). As discussed by Dendukuri et al. [11], since oxygen diffusion in PDMS is two orders of magnitude faster than in PEG-DA, oxygen can be taken to be flowing freely in PDMS and therefore the cross-section in contact with PDMS was open to oxygen during reaction. In the comparison group, a glass barrier was inserted to block oxygen (Fig. 1(c)). After curing the first part, the barrier was removed, and the resin was injected into the second half of the mold. The whole structure with a total length of 15 mm was then cured for a prescribed sufficiently long time (Fig. 1(c)). The cured sample was cut into a 15 mm × 4 mm × 1 mm strip with the interface at the center. Tensile tests in the direction perpendicular to the interface were carried out by using a dynamic mechanical analysis (DMA) tester (Q800, TA Instruments, New Castle, DE, USA) in Control Force mode. In order to test the mechanical behavior of normal PEG-DA sample without interface, bulk strips (15 mm × 4 mm × 1 mm) are cured with an intensity of 3.5 mW cm^{-2} and an irradiation time of 15 min. The interface was characterized on a scanning electron microscope (SEM) (LEO 1530, ZEISS, Oberkochen, Germany) and a trinocular microscope (89404-886, VWR, Suwanee, GA). Fourier transform infrared (FT-IR) spectrum of the sample surface was taken on an FT-IR spectrometer (Nicolet iS50, Thermo Scientific, Waltham, MA, USA) with an attenuated total reflection (ATR) unit.

2.2. Experimental results

SEM and microscopic images of the interfacial structures are shown in Fig. 2. In these figures, the locations of the interfaces are identified by the ridges and are marked by thin dashed lines. It is clear there are no apparent discontinuities, such as voids or cracks, at the interfaces, regardless of whether the first part was covered by PDMS or by glass. Thus the interface in this work is different from those created by pressure or heating, as in, for example, the work of Jud and Brown [21,22]. This is a reasonable result because the interfacial structure was developed through curing the liquid resin against a solid surface. Conventional fracture tests of interfaces [23] may not be reliable for this continuous interphase. Furthermore, the brittle nature of crosslinked PEG-DA makes it difficult to examine with peeling or lap shear tests [24].

Fig. 3(a) shows stress–strain curves of four samples prepared under the same condition (using PDMS barrier, with light intensity 3.5 mW cm^{-2}, first curing time of 5 min, second curing time of 15 min). All four samples broke at the interfaces. Fig. 3(b) shows stress–strain curves of normal bulk samples without interface. Comparing to Fig. 3(a), it is clear that the strength of cured polymer decreases significantly due to the presence of an interface. The same tensile experiments were conducted on samples prepared under different conditions. Fig. 3(c) summarizes the results of the tensile strength as a function of first curing time; the samples in this group had the same second curing time of 15 min and the same curing irradiation intensity of 3.5 mW cm^{-2} for both parts. In Fig. 3(c), each experimental point is averaged from at least four tests. Two observations can be made based on these results. First, the interfacial strength decreases with the curing time of the first part. Second, the existence of oxygen can improve the interfacial strength, especially for longer curing times. The first observation is easy to understand. Strong interfacial bonding depends on the development of sufficient interfacial bridging bonds as well as surface roughness. For a flat interface (as in our case), the former will certainly play a major role. As the curing degree of the first part increases with the irradiation time, there are fewer unreacted double bonds at the surface. As a result, interfacial bridging with the second part becomes more difficult, which finally leads to a weaker interfacial strength. The second finding coincides with those of Dall'Oca et al. [17]. When a sample is open to air, the number of radicals in a thin surface layer is significantly reduced due to oxygen inhibition, and the conversion of double bonds by radicals is decelerated. Therefore, even if the material beneath the surface is well cured, there are still many unreacted double bonds left near surface. An indication of this phenomenon is the tacky nature of

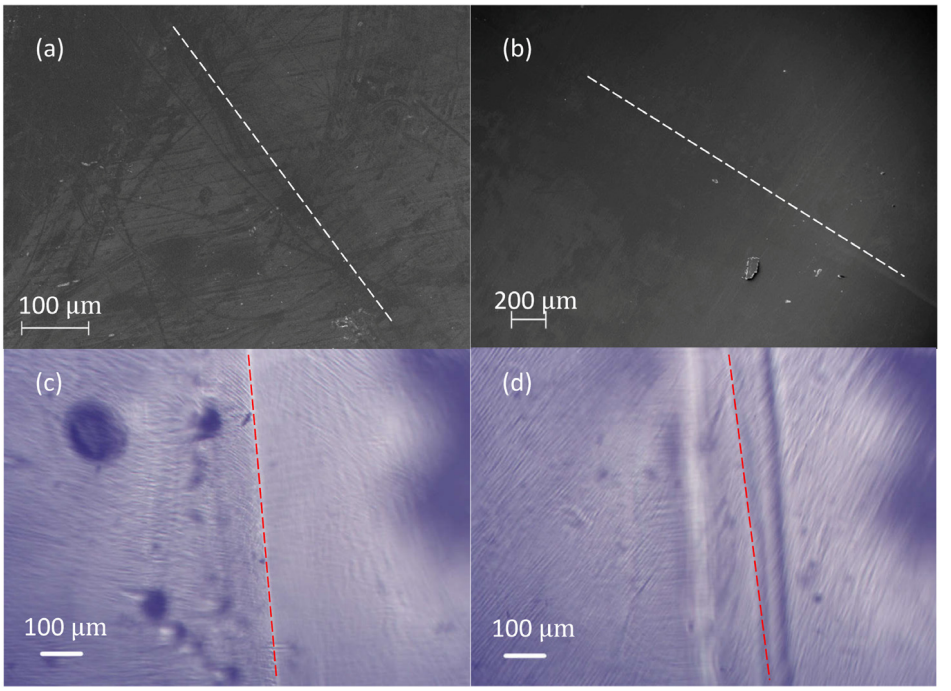

Fig. 2. SEM and optical micrographs of the interface. (a) SEM image of sample interface prepared by inserting a glass barrier. (b) SEM image of sample prepared by inserting a PDMS barrier. (c) Microscopic image of sample interface prepared by inserting a glass barrier. (d) Microscopic image of sample interface prepared by inserting a PDMS barrier. (Dashed lines were added to indicate the position of interface.)

the surface layer [13]. These unreacted double bonds act as potential sites for interfacial bridging once a second layer of resin is poured on the surface of the first. This explains why structures open to air show higher interfacial strength.

The existence of unconverted double bonds is verified from the surface FT-IR spectrum of the first part (Fig. 3(d)). The absorbance peak at 810 cm^{-1}, corresponding to the twisting vibration of CH_2=CH bonds [25], is chosen as an indicator of reaction. This peak decreases with the consumption of double bonds in acrylates [26]. The curves in Fig. 3(d) are normalized by the peak around 1725 cm^{-1} for C=O bonds, which should not change during photopolymerization [26]. After 2 min irradiation, as a result of photopolymerization, the double bond peak becomes very small for a surface covered by glass, but the same peak is still very strong for a surface covered by PDMS, indicating a large number of unconverted double bonds. After 10 min irradiation, the double bond peak for the surface covered by PDMS is still apparent, but it almost disappears for the case covered by glass.

A second set of experiments was conducted by varying the light intensity while holding the curing time of the first part at 2 min and the second curing time at 15 min. Although the presence of oxygen improves interfacial behavior even if light intensity reaches 15 mW cm^{-2}, the interfacial strength shows a continuous decrease with increases in light intensity (Fig. 3(e)). Photoinitiators certainly break into radicals at a faster rate at a higher light intensity, which means that under high intensity conditions there are fewer unconverted double bonds after a given time period. As a result, interfacial bridging with the second part becomes harder, as there are fewer active sites on the first part. Oxygen can only slow this tendency, thus it can improve the interfacial strength. Increasing light intensity is a strategy frequently used to reduce the oxygen inhibition effect during photopolymerization [10]; but it does not work well in improving interfacial bonding. Since a higher light intensity is desirable in the case of fast curing, exposing the surface layer to oxygen is a feasible method to improve interfacial properties at the same time.

3. Modeling interfacial strength

It was shown experimentally in Section 2 that oxygen inhibition can increase interfacial strength during part-by-part photopolymerization. But the extent to which oxygen may improve interfacial properties depends on several processing parameters, such as irradiation intensity, oxygen concentration and resin composition. This section presents a theoretical model that can capture the effect of oxygen under these different conditions. The model is mainly based on classical methods used in previous work on photochemistry [5,8,11] and on photmechanics [27–30], but several additional assumptions are introduced to further simplify the model.

Fig. 4 shows the configuration of the problem. In the samples we prepared, the total length $2L$ along the x-axis is sufficiently large that we have $h \ll L$ and $w < L$. We start from reactions in the first part ($x < 0$ in Fig. 4), which will be in contact with the second part. The concentrations of chemical species at $x > 0$ are set to zero during the first curing. The first assumption is that light attenuation along the sample thickness can be ignored. This is because

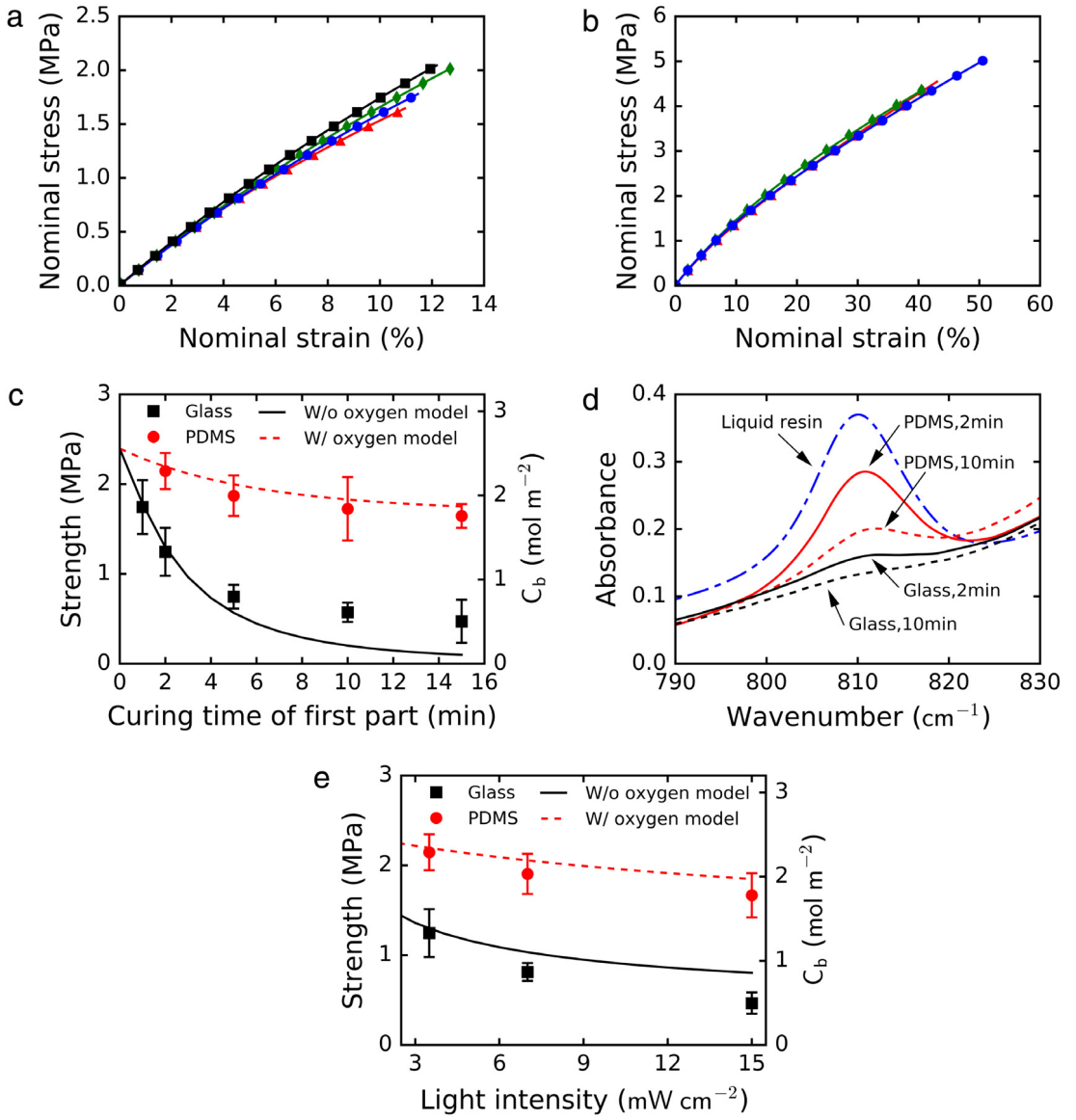

Fig. 3. Selected tensile curves of samples (inserting PDMS barrier, light intensity 3.5 mW cm^{-2}, curing time of first part 5 min). (b) Tensile curves of 3 normal samples without interface (light intensity 3.5 mW cm^{-2}, curing time 15 min). (c) Symbols: Tensile strength as a function of curing times for the first part (light intensity 3.5 mW cm^{-2}); Lines: concentration of interfacial bridges as a function of first part curing time (from the model in Section 3). (d) FT-IR spectrum of liquid PEG-DA resin, the surface of the first part covered by glass or PDMS after 2 min irradiation and after 10 min irradiation. (Incident light intensity 3.5 mW cm^{-2}). (e) Symbols: Tensile strength as a function of light intensity (curing time of first part 2 min); Lines: concentration of interfacial bridges as a function of light intensity (from the model in Section 3).

h is relatively small and we are interested in interfaces that are parallel to the irradiation. The concentrations of photoinitiators, radicals, interfacial bonds, etc., are taken as averages across the thickness, and they will only be functions of time and coordinates x and y. In addition, it is reasonable to assume that the irradiation is uniform in the sample plane, because the sample's dimensions are smaller than the size of the light projection. A non-uniform field could only be created from boundary effects along the x-axis. Therefore, all the quantities are functions of time and x only. The evolution of photoinitiator concentration $\tilde{C}_I$ is described as,

$$\frac{\partial \tilde{C}_I(x,t)}{\partial t} = \underbrace{-\beta \tilde{C}_I(x,t) I_0}_{\textit{photoinitiator consumption}} + \underbrace{D_I \frac{\partial^2 \tilde{C}_I(x,t)}{\partial x^2}}_{\textit{photoinitiator diffusion}} . \quad (1)$$

Here β is a reaction parameter, I_0 is the incident light intensity and t is the irradiation time of the first part. Here, a tilde ($\sim$) is added to the top of C_I to indicate that it is a state variable for the first curing, and so for the other state variables used for the first curing. The first term on the right-hand side (RHS) of Eq. (1) represents

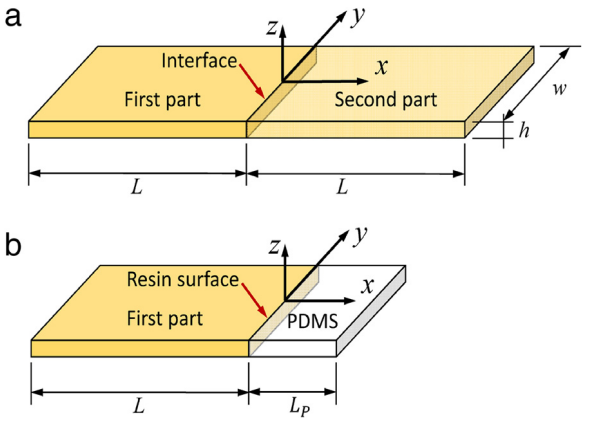

Fig. 4. Schematic graphs of the modeling domains of whole sample (a) and first part curing (b).

the consumption of photoinitiators upon irradiation. A Fickian diffusion term is introduced in the RHS of Eq. (1) to account for the motion of photoinitiators triggered by oxygen inhibition. The initial photoinitiator concentration, which will be written as C_{I0} afterwards, can be obtained from the resin composition. The boundary condition for Eq. (1) is simply set as $\frac{\partial \tilde{C}_I(x,t)}{\partial x}\Big|_{x=-L} = \frac{\partial \tilde{C}_I(x,t)}{\partial x}\Big|_{x=0} = 0$.

Primary radicals are created by the cleavage of photoinitiators, and subsequently are transferred to propagating radicals. Here all types of reactive radicals except peroxy radicals are considered the same, which is the case in many previous works [8,11]. Thus the evolution of radical concentration $\tilde{C}_R$ is written as [14],

$$\frac{\partial \tilde{C}_R(x,t)}{\partial t} = \underbrace{2\beta \tilde{C}_I(x,t)}_{\text{radical generation}} - \underbrace{k_t \tilde{C}_R^2(x,t)}_{\text{self-termination}} - \underbrace{k_o \tilde{C}_R(x,t)\tilde{C}_o(x,t)}_{\text{oxygen inhibition}}. \quad (2)$$

The first term on the RHS of Eq. (2) represents the creation of radicals. In comparison with the RHS of Eq. (1), a factor of 2 is introduced to account for the fact that one photoinitiator always cleaves into two radicals. The second and third terms on the RHS of Eq. (2) describes the self-termination and oxygen inhibition, respectively. k_t and k_0 are two reaction constants. Because peroxyl radicals created through inhibition are less active and are very easy to terminate, they are ignored in the subsequent reactions. In the cases studied here, there is a gradient of radical concentration near the interface (from the interface to the inside of the sample). But the diffusivity of radicals is relatively slow, as they quickly attach to polymer chains. We therefore neglect the diffusion of radicals in the above equation. The initial value of $\tilde{C}_R$ in Eq. (2) is set to $\tilde{C}_R(x,0) = C_{R0} = 0$ because there are no radicals at the beginning of the reactions [5].

The evolution of oxygen obeys a similar rule, as shown in our previous work [14],

$$\frac{\partial \tilde{C}_o(x,t)}{\partial t} = -\underbrace{k_o \tilde{C}_R(x,t)\tilde{C}_o(x,t)}_{\text{oxygen consumption}} + \underbrace{D_{o\text{-}PEGDA}\frac{\partial^2 \tilde{C}_o(x,t)}{\partial x^2}}_{\text{oxygen diffusion}}. \quad (3)$$

The first term on the RHS of Eq. (3) indicates oxygen consumption during the inhibition reaction, while the second term describes the Fickian diffusion of oxygen. The initial value of $\tilde{C}_o$ in $x < 0$ is set to the equilibrium oxygen concentration in PEG-DA, which can be obtained from Henry's law [31] as $C_{o0} = S_{o\text{-}PEGDA}P_o$. Here $S_{o\text{-}PEGDA}$ is the solubility of oxygen in PEG-DA and P_o is the partial pressure of atmospheric oxygen. Because the side far from the free surface is blocked from oxygen, a no flux boundary condition $\frac{\partial \tilde{C}_o(x,t)}{\partial x}\Big|_{x=-L} = 0$ is used. For the case without oxygen, the boundary condition at $x = 0$ is also set to $\frac{\partial \tilde{C}_o(x,t)}{\partial x}\Big|_{x=0} = 0$. For the case with oxygen (using PDMS), an additional domain is introduced for the evolution of oxygen if the surface of the first part is covered by PDMS with a thickness of L_P (Fig. 4(b)). Oxygen transportation in the PDMS barrier is described as,

$$\frac{\partial \tilde{C}_o(x,t)}{\partial t} = D_{o\text{-}PDMS}\frac{\partial^2 \tilde{C}_o(x,t)}{\partial x^2}, \quad (4)$$

where $D_{o\text{-}PDMS}$ is the oxygen diffusivity in PDMS. The initial value of $\tilde{C}_o$ in $0 < x < L_P$ and the boundary value of $\tilde{C}_o$ at the surface open to air ($x = L_P$) are set to the equilibrium oxygen concentration in PDMS, which can be obtained from $C_{o\text{-}PDMS} = S_{o\text{-}PDMS}P_o$. Here $S_{o\text{-}PDMS}$ is the solubility of oxygen in PDMS. The continuities of diffusion flux and oxygen partial pressure across the PEG-DA/PDMS interface ($x = 0$) are controlled by $D_{o\text{-}PEGDA}\frac{\partial \tilde{C}_o(x,t)}{\partial x}\Big|_{x=0^-} = D_{o\text{-}PDMS}\frac{\partial \tilde{C}_o(x,t)}{\partial x}\Big|_{x=0^+}$ and $\frac{\tilde{C}_o(0^-,t)}{S_{o\text{-}PEGDA}} = \frac{\tilde{C}_o(0^+,t)}{S_{o\text{-}PDMS}}$, respectively [32]. $x = 0^-$ indicates the first part side and $x = 0^+$ means the PDMS side.

During the chain propagation, the double bonds are cleaved and transferred to propagating radicals. The number of radicals remains the same in this process, but the concentration of unconverted double bonds will obey the following kinetics,

$$\frac{\partial \tilde{C}_M(x,t)}{\partial t} = \underbrace{-k_p \tilde{C}_M(x,t)\tilde{C}_R(x,t)}_{\text{double bonds consumption}}. \quad (5)$$

Here $\tilde{C}_M$ represents the concentration of double bonds in the crosslinkers, and k_p is a reaction constant of propagation. The RHS of Eq. (5) implies the consumption of double bonds by radicals. The initial value of $\tilde{C}_M$, which is written as $\tilde{C}_{M0}$, can be obtained from the resin composition.

We now turn to the curing of the second part. Here, we consider the scenario where the first part, after being cured for a period t_1, comes in contact with the second part, which is pure unreacted resin. Upon contact, the whole interface area is blocked from atmospheric oxygen. The evolution of chemical species in the two separate parts will obey same rules outlined in Eqs. (1)–(3) and (5), but the domain of these equations is changed to the whole sample plane ($-L < x < L$, Fig. 4), i.e.,

$$\frac{\partial C_I(x,\tau)}{\partial \tau} = -\beta C_I(x,\tau)I_0 + D_I\frac{\partial^2 C_I(x,\tau)}{\partial x^2}, \quad (6a)$$

Table 1
Parameters in the model.

Parameters	Value	Description and reference
C_{I0} (mol L^{-1})	0.02	Photoinitiator concentration (calculated)
C_{M0} (mol L^{-1})	3.2	Double bonds concentration (calculated)
$S_{o\text{-}PEGDA}$ (cm^3(*STP*)/cm^3 atm)	0.1	Oxygen solubility in PEG-DA [10]
$S_{o\text{-}PDMS}$ (cm^3(*STP*)/cm^3 atm)	0.46	Oxygen solubility in PDMS [38]
P_o (atm)	0.21	Atmospheric oxygen partial pressure
C_{o0} (mol L^{-1})	0.001	Equilibrium oxygen concentration in PEG-DA [10]
$C_{o\text{-}PDMS}$ (mol L^{-1})	0.004	Equilibrium oxygen concentration in PDMS [38]
D_I (m^2 s^{-1})	1×10^{-10}	Photoinitiator diffusivity [36]
$D_{o\text{-}PEGDA}$ (m^2 s^{-1})	1×10^{-11}	Oxygen diffusivity in PEG-DA [39]
$D_{o\text{-}PDMS}$ (m^2 s^{-1})	3.4×10^{-9}	Oxygen diffusivity in PDMS [38]
L_P (mm)	0.5	PDMS barrier thickness (measured)
β (cm^2 mW^{-1} s^{-1})	7×10^{-4}	Photoinitiation coefficient [14]
k_t (L mol^{-1} s^{-1})	1×10^{6}	Self-termination coefficient [36]
k_o (L mol^{-1} s^{-1})	7×10^{4}	Oxygen inhibition coefficient [4]
k_p (L mol^{-1} s^{-1})	6×10^{2}	Propagation coefficient [36]
k_b (cm^4 mol^{-1} s^{-1})	300	Interfacial bridging coefficient
α (MPa m^2 mol^{-1})	0.94	Scaling factor of strength (calculated)

$$\frac{\partial C_R(x,\tau)}{\partial \tau} = 2\beta C_I(x,\tau) - k_t C_R^2(x,\tau) - k_o C_R(x,\tau) C_o(x,\tau), \tag{6b}$$

$$\frac{\partial C_o(x,\tau)}{\partial \tau} = -k_o C_R(x,\tau) C_o(x,\tau) + D_{o\text{-}PEGDA}\frac{\partial^2 C_o(x,\tau)}{\partial x^2}, \tag{6c}$$

$$\frac{\partial C_M(x,\tau)}{\partial \tau} = -k_p C_M(x,\tau) C_R(x,\tau). \tag{6d}$$

To prevent confusion, we replace t by τ (so that $\tau = t - t_1$) as the cure time after the two parts are in contact. The initial condition for the second curing in the whole domain should be,

$$\begin{cases} C_i(x,0) = \tilde{C}_i(x,t_1), & (x \le 0) \\ C_i(x,0) = C_{i0}, & (x > 0) \end{cases} \quad (i = I, R, o, M), \tag{7}$$

where C_{i0} indicates the initial value of different species prior to the reaction. The boundary conditions for Eqs. (6a) and (6c) are,

$$\left.\frac{\partial C_i(x,\tau)}{\partial x}\right|_{x=\pm L} = 0, \quad (i = I, o). \tag{8}$$

The final step deals with the interfacial bridging between these two surface layers. Here, a key assumption is that the rate of interfacial bonding is proportional to the amount of unconverted double bonds in both sides, which is similar to Fredrickson et al. [33] and O'Shaughnessy et al. [34]. Therefore,

$$\frac{dC_b(\tau)}{d\tau} = k_b C_M(0^-,\tau) C_M(0^+,\tau)\frac{\left(C_R(0^-,\tau)+C_R(0^+,\tau)\right)}{2}, \tag{9}$$

where C_b is concentration of bridging chains per unit area (mol m^{-2}), and k_b is a reaction constant of bridging. $x = 0^-$ indicates the first part side and $x = 0^+$ means the second part side. Interfacial bridging actually results from chain propagation, and thus the rate of it should also be proportional to the amount of free radicals near interface. An average of free radical concentration in two sides is used in Eq. (9). The correlation between C_b and the interfacial tensile strength σ_s is straight forward by applying the simple relation proposed by Vincent et al. [35], that is $\sigma_s = \alpha C_b$ where α is a scaling factor.

4. Numerical results and discussions

In this section, results based on the theoretical model are presented. Equations in Section 3 were solved numerically to obtain the value of the interfacial chain concentration, C_b. Parameters used in the model are listed in Table 1. Although diffusivities of chemical species may change during the reaction process [36], they are set to constant values in the model. This will not lead to significant deviations as shown by Dendukuri et al. [11] and Long et al. [37]. It should be noted that although k_b and α have their specific physical meanings, their contributions can be lumped into one parameter $k_b\alpha$. In the current work, we set k_b to a value so that the magnitude of C_b is comparable to C_M and the interfacial bond density will be comparable to the chain density of the bulk material. Then the scaling factor α is selected by comparing the model with experiments, which will be shown later.

The evolution of chemical species during the first and the second curing are respectively shown in Fig. 5(a)–(c) and (d)–(e). As shown in Fig. 5(a), in the curing of the first part, although initially there are residual oxygen molecules inside the resin, they are consumed quickly. For the case of using PDMS barrier, oxygen mainly aggregates in a thin layer near the face that is in contact with PDMS. Because the diffusivity of oxygen in PDMS is two orders of magnitude higher than that in PEG-DA, the oxygen concentration at the resin surface ($x = 0$) nearly remains the same during the reaction (Fig. 5(b)). This is true even if the thickness of the PDMS barrier L_P approaches 2 mm. Fig. 5(b) shows that the PDMS serves as an oxygen reservoir, which continuously pumps oxygen into the PEG-DA. In addition, it is only the oxygen in the PEG-DA affects the reaction, and the oxygen content in the PDMS is much higher than that in the PEG-DA; therefore, in regard to the effects of oxygen to the radical depletion, PDMS is

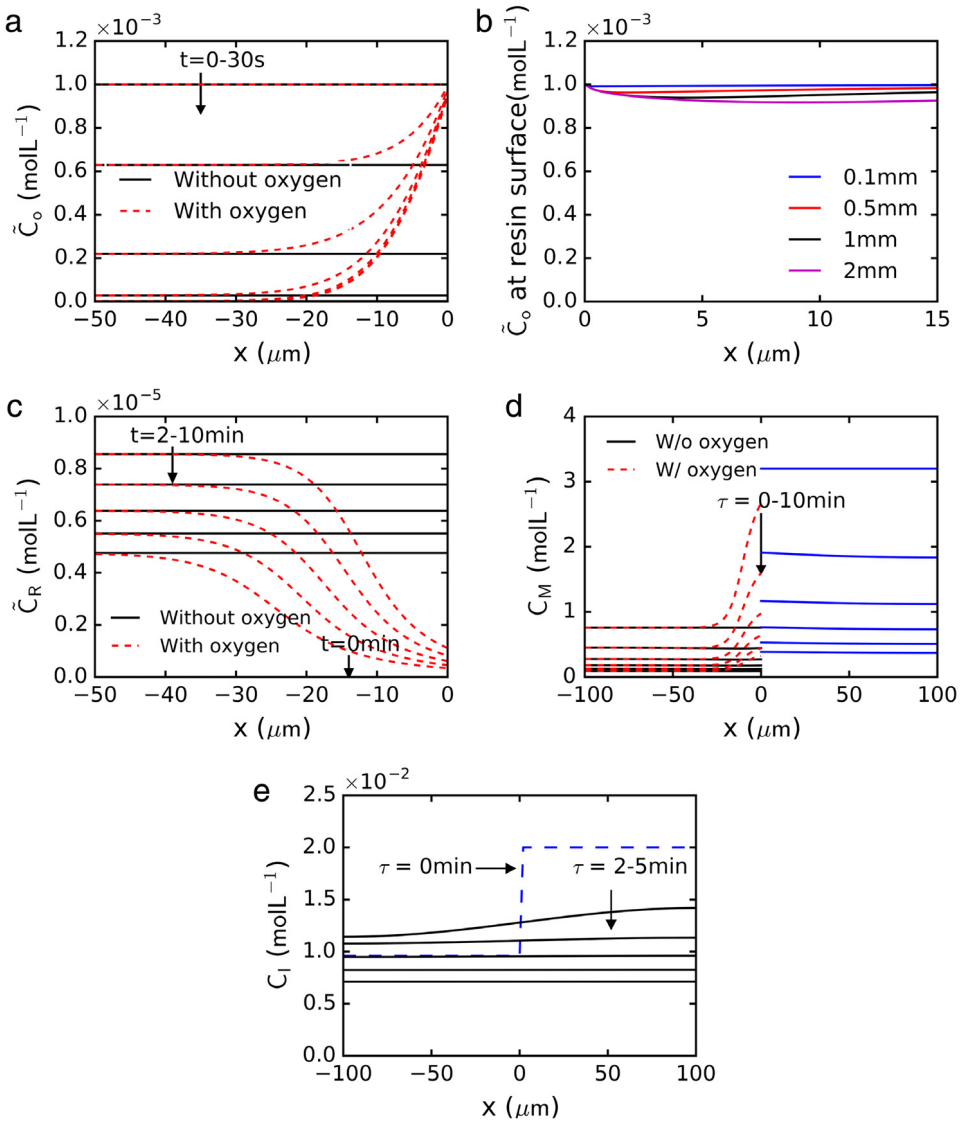

Fig. 5. Evolution of different species during the part-by-part curing. (a) Oxygen concentration near the interface during the first part curing. (b) Oxygen concentration at resin surface as a function of time and PDMS barrier thickness. (c) Radical concentration near the free surface during the first part curing. (d) Double bond concentration in two sides during the second part curing (the first part curing time is 5 min). (e) Photoinitiator concentration across the interface during the second part curing (the first part curing time is for 5 min). (Incident light intensity for (a)–(e) 3.5 mW cm^{-2}.)

the same as open air. In the vicinity of this surface layer where oxygen inhibition dominates the reaction process, the number of reactive radicals is significantly reduced (Fig. 5(c)). As a result, the conversion of double bonds near the surface is reduced, which provides more unreacted sites for interfacial bridging upon contact with the second part (Fig. 5(d)). It should also be noted that as the second part resin is brought into contact with the first part, photoinitiators diffuse into the first part, which helps to further cure the first part. Fig. 5(e) shows the diffusion of photoinitiators from the second part to the first part as a result of the concentration gradient. This also accelerates double bond conversion in the first part and contributes to interfacial reaction with the second part.

The evolution of C_b based on Eq. (9) is shown in Fig. 3(c) and (e) as lines. The scaling factor α between the interfacial bridge concentration C_b and the interfacial strength σ_s is set to be 3 (MPa)/3.2 (mol m^{-2}) = 0.94 (MPa m^2 mol^{-1}). The results obtained using the theoretical model agree well with the experimental results. The interfacial strength shows a continuous reduction with both the irradiation time and the light intensity, as a result of a decrease in the number of double bonds in the first part, which is shown in Fig. 6(a)–(b). This trend is decelerated if oxygen is present. Because radicals are significantly reduced through inhibition reaction (Fig. 5(b)), many more double bonds are left unconverted (Fig. 5), which is beneficial to interfacial bridging with the second part. In Fig. 3(c), for the case without oxygen, deviations between model prediction and experiments appear at longer time intervals. This may be because self-termination no longer obeys a second order kinetic rule due to the entanglement effect of the network.

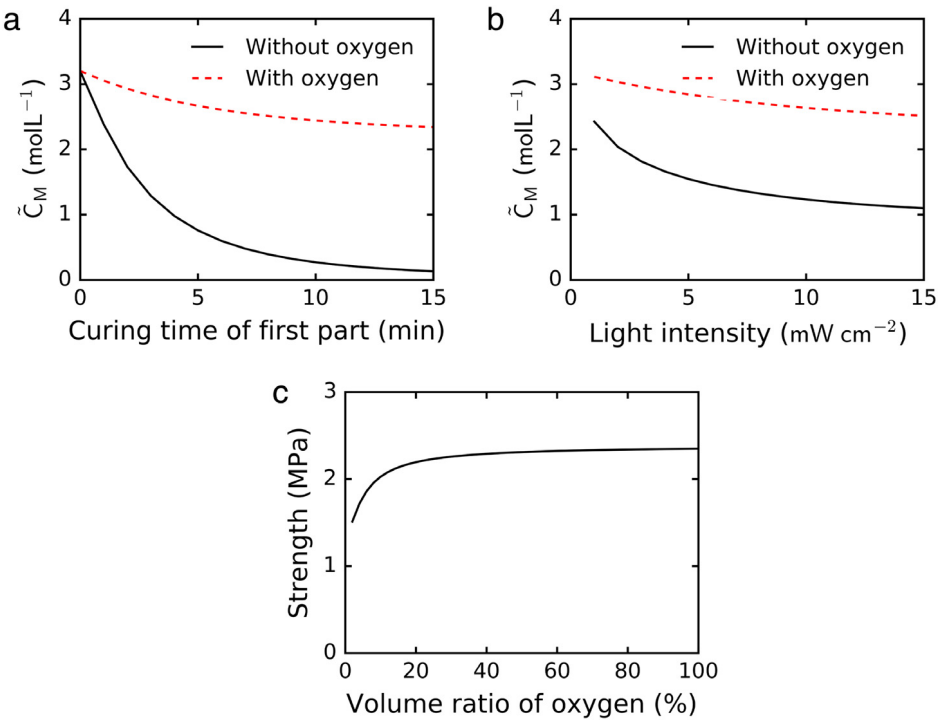

Fig. 6. (a) Double bond concentration near the surface as a function of first part curing time (incident light intensity $I_0 = 3.5$ mW cm^{-2}). (b) Double bond concentration near the surface as a function of incident light intensity (first part curing time 2 min). (c) Interfacial strength as a function of atmospheric oxygen volume ratio (first part cured for 2 min, $I_0 = 3.5$ mW cm^{-2}).

The deviations in Fig. 3(c) and (e) for the case with oxygen may occur simply because we neglect the effect of surface roughness. As the cured PEG-DA surface covered by PDMS is slightly rougher than the one covered by glass, this may also contribute to interfacial strength improvement.

In order to better illustrate the role of oxygen, interfacial bridging is calculated by varying the volume ratio of atmospheric oxygen; the interfacial strength is then derived by using the scaling relation $\sigma_s = \alpha C_B$. As can be seen in Fig. 6(c), interfacial strength σ_s increases by almost 50% as the atmosphere approaches pure oxygen. The strength as oxygen volume ratio approaches 0 corresponds to the case without oxygen.

We then conduct parametrical studies by varying model parameters. Here, the strengths of interfaces with (σ_s^{with}) and without oxygen ($\sigma_s^{without}$) are calculatedrespectively. Fig. 7(a)–(b) show the dependence of $\sigma_s^{with} - \sigma_s^{without}$ on resin composition, specifically the initial photoinitiator concentration C_{I0} and the initial double bond concentration C_{M0}. The red dot in Fig. 7(a) indicates the experimental condition in Section 2. As shown in both Fig. 7(a) and (b), the effect of oxygen is more apparent with the increase of C_{M0} at a fixed C_{I0}. This trend can also be found in Fig. 7(c). According to Eqs. (5) and (6d), the conversion rate of double bonds is proportional to a product of C_M and C_R, which relate to C_{M0} and C_{I0}, respectively. For a constant initial photoinitiator concentration, increasing the number of double bonds implies that more double bonds will be left unreacted. This is more pronounced in the presence of oxygen at the interface, as oxygen consumes a significant number of radicals. This analysis can also be used to explain Fig. 7(d) where the initial photoinitiator concentration increases while maintaining the double bond concentration constant. In this case, the increase of photoinitiators generates more radicals, which consume more double bonds at the interface and thus reduce the interfacial strength. However, if the number of photoinitiator is too small, as the leftmost edge in Fig. 7(d), photopolymerization cannot even start and the interfacial strength drops to zero. Fig. 7(a)–(d) suggest that a resin composed of a relatively small number of photoinitiators and a large number of double bonds (which can be realized by using short chain crosslinkers [40]) seems desirable for the interfacial strength of incrementally photopolymerized structures.

The discussion of Fig. 7 shows that the conversion rate of double bonds plays an important role in determining the interfacial strength. In general, a slow conversion rate of double bonds at the interface in the first part curing will lead to a stronger interface. However, a slow double bond conversion rate in the bulk, which can be controlled by the photoinitiator concentration and the initial double concentration, is not desirable in layer-by-layer applications, as this leads a condition where the whole material/structure fails to fully cure. Oxygen, which only dominates at the interface, provides an efficient method of reducing the double bond conversion rate at the interface, thus it is beneficial to the interfacial strength and to the overall properties of the part or structure.

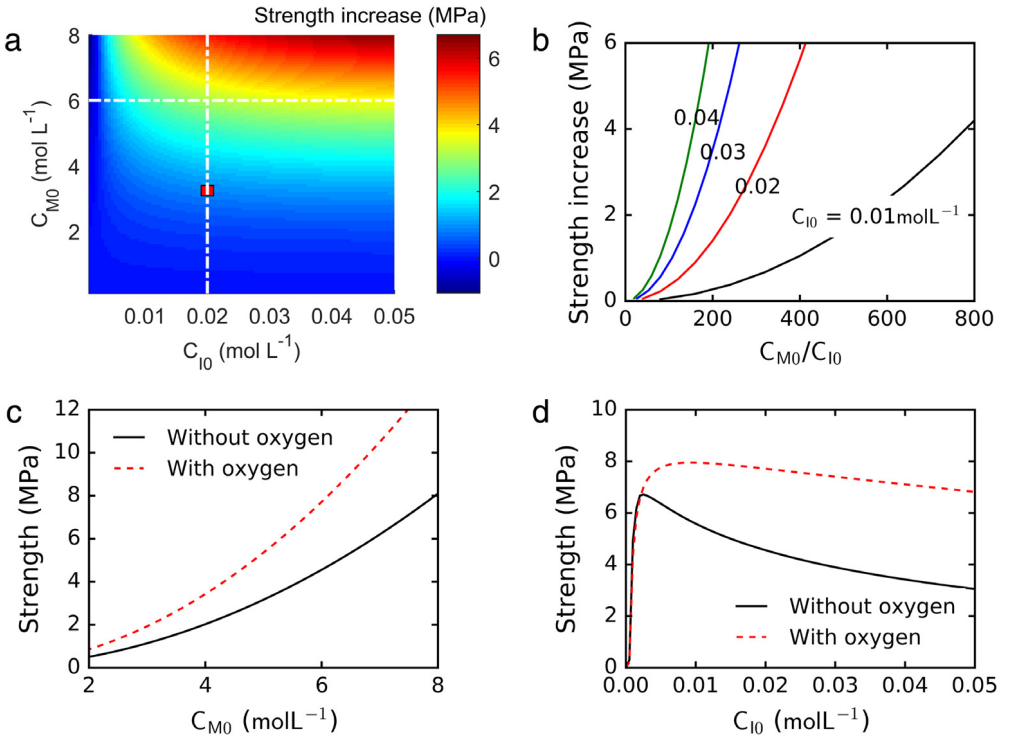

Fig. 7. (a) Strength increase due to oxygen as a function of initiator concentration C_{I0} and double bond concentration of C_{M0} (first part cured for 2 min, incident light intensity 3.5 mW cm^{-2}). (b) Strength increase due to oxygen as a function of C_{M0}/C_{I0} (extracted from (a)). (c) Interfacial strength as a function of double bond concentration C_{M0} (C_{I0} = 0.02 mol L^{-1}, extracted from (a)). (d) Interfacial strength as a function of initiator concentration C_{I0} (C_{M0} = 6 mol L^{-1}, extracted from (a)). (For interpretation of the references to color in this figure legend, the reader is referred to the web version of this article.)

5. Conclusion

In this paper, we studied the effects of oxygen on interfacial properties in incremental photopolymerization. We found experimentally that in a part-by-part photopolymerization cured structure, interfacial strength decreases with curing time and incident light intensity of the first part, while the presence of oxygen can significantly improve the strength of the interface. The role of oxygen becomes much more apparent if the first part of an interfacial structure is cured for a long time. The improvement of interfacial strength is attributed to the fact that chain propagation and thus double bond consumption at the surface layer will be decelerated if the amount of radical is reduced by oxygen inhibition. Unconverted double bonds in the first part are beneficial for interfacial bonding with a second part. Based on these results, we proposed a model that can capture the evolution of interfacial bridging and interfacial strength very well. Several numerical simulations were carried out using the theoretical model, and the role of processing parameters such as oxygen concentration and resin components were investigated based on the details of chemical reactions. It was found the interfacial strength increases with atmospheric oxygen concentration. We also found that interfaces with improved strength can be obtained by either decreasing the amount of photoinitiator or by using short chain crosslinkers that can increase the concentration of double bonds.

Acknowledgments

We acknowledge the support of the NSF award (CMMI-1462895) and an AFOSR grant (FA9550-13-1-0088; Dr. B.-L. "Les" Lee, Program Manager). Z.Z. acknowledges a support from Chinese Scholarship Council (201506010219). The usage of material characterization facilities in the Institute of Electronic and Nanotechnology at Georgia Institute of Technology is also acknowledged.

References

[1] C. Decker, The use of UV irradiation in polymerization, Polym. Int. 45 (2) (1998) 133–141.
[2] J.-P. Fouassier, Photoinitiation, Photopolymerization, and Photocuring: Fundamentals and Applications, Hanser, 1995.
[3] I. Gibson, D.W. Rosen, B. Stucker, Additive Manufacturing Technologies, Springer, New York, 2010.
[4] G. Odian, Principles of Polymerization, John Wiley & Sons, 2004.
[5] C. Decker, A.D. Jenkins, Kinetic Approach of O-2 Inhibition in Ultraviolet-Induced and Laser-Induced Polymerizations, Macromolecules 18 (6) (1985) 1241–1244.
[6] C. Decker, Kinetic study and new applications of UV radiation curing, Macromol. Rapid Commun. 23 (18) (2002) 1067–1093.
[7] A.K. O'Brien, C.N. Bowman, Impact of oxygen on photopolymerization kinetics and polymer structure, Macromolecules 39 (7) (2006) 2501–2506.
[8] A.K. O'Brien, C.N. Bowman, Modeling the effect of oxygen on photopolymerization kinetics, Macromol. Theory Simul. 15 (2) (2006) 176–182.
[9] A.S. Jariwala, et al., Modeling effects of oxygen inhibition in mask-based stereolithography, Rapid Prototyp. J. 17 (3) (2011) 168–175.
[10] S.C. Ligon, et al., Strategies to reduce oxygen inhibition in photoinduced polymerization, Chem. Rev. 114 (1) (2014) 557–589.

[11] D. Dendukuri, et al., Modeling of oxygen-inhibited free radical photopolymerization in a PDMS microfluidic device, Macromolecules 41 (22) (2008) 8547–8556.
[12] H.E. Jeong, et al., UV-assisted capillary force lithography for engineering biomimetic multiscale hierarchical structures: From lotus leaf to gecko foot hairs, Nanoscale 1 (3) (2009) 331–338.
[13] M. Guvendiren, S. Yang, J.A. Burdick, Swelling-induced surface patterns in hydrogels with gradient crosslinking density, Adv. Funct. Mater. 19 (19) (2009) 3038–3045.
[14] Z.A. Zhao, et al., Effects of oxygen on light activation in covalent adaptable network polymers, Soft Matter 11 (30) (2015) 6134–6144.
[15] J.R. Tumbleston, et al., Continuous liquid interface production of 3D objects, Science 347 (6228) (2015) 1349–1352.
[16] H.E. Jeong, K.Y. Suh, On the role of oxygen in fabricating microfluidic channels with ultraviolet curable materials, Lab Chip 8 (11) (2008) 1787–1792.
[17] S. Dall'Oca, et al., Effect of oxygen inhibition on composite repair strength over time, J. Biomed. Mater. Res., Part B 81B (2) (2007) 493–498.
[18] D. Truffier-Boutry, et al., Interfacial layer characterization in dental composite, J. Oral Rehabil. 30 (1) (2003) 74–77.
[19] J.S. Kim, et al., Effect of light-cure time of adhesive resin on the thickness of the oxygen-inhibited layer and the microtensile bond strength to dentin, J. Biomed. Mater. Res., Part B 78B (1) (2006) 115–123.
[20] E.S. Shawkat, et al., Oxygen inhibition and incremental layer bond strengths of resin composites, Dent. Mater. 25 (11) (2009) 1338–1346.
[21] K. Jud, H.H. Kausch, J.G. Williams, Fracture-Mechanics Studies of Crack Healing and Welding of Polymers, J. Mater. Sci. 16 (1) (1981) 204–210.
[22] H.R. Brown, Relation between the width of an interface between two polymers and its toughness, Macromolecules 34 (11) (2001) 3720–3724.
[23] D.A. Dillard, A.V. Pocius, Adhesion Science and Engineering: The Mechanics of Adhesion, Elsevier, 2002.
[24] K.L. Mittal, K.-W. Lee, Polymer Surfaces and Interfaces: Characterization, Modification and Application, VSP, 1997.
[25] H.Q. Lin, et al., The effect of cross-linking on gas permeability in cross-linked poly(ethylene glycol diacrylate), Macromolecules 38 (20) (2005) 8381–8393.
[26] S. Kalakkunnath, et al., Viscoelastic characteristics of UV polymerized poly(ethylene glycol) diacrylate networks with varying extents of crosslinking, J. Polym. Sci. Part B 44 (15) (2006) 2058–2070.
[27] K. Long, et al., Photomechanics of light-activated polymers, J. Mech. Phys. Solids 57 (7) (2009) 1103–1121.
[28] K.N. Long, et al., Photo-induced deformation of active polymer films: Single spot irradiation, Internat. J. Solids Structures 48 (14–15) (2011) 2089–2101.
[29] R. Long, H.J. Qi, M.L. Dunn, Thermodynamics and mechanics of photochemcially reacting polymers, J. Mech. Phys. Solids 61 (11) (2013) 2212–2239.
[30] J. Ma, et al., A photoviscoplastic model for photo activated covalent adaptive networks, J. Mech. Phys. Solids 70 (2014) 84–103.
[31] S.A. Stern, S. Trohalaki, Fundamentals of gas-diffusion in rubbery and glassy-polymers, in: W.J. Koros (Ed.), Barrier Polymers and Structures, American Chemical Society, 1990, pp. 22–59.
[32] L. Poulsen, et al., Oxygen diffusion in bilayer polymer films, J. Phys. Chem. B 107 (50) (2003) 13885–13891.
[33] G.H. Fredrickson, S.T. Milner, Time-dependent reactive coupling at polymer–polymer interfaces, Macromolecules 29 (23) (1996) 7386–7390.
[34] B. O'Shaughnessy, D. Vavylonis, Reactive polymer interfaces: How reaction kinetics depend on reactivity and density of chemical groups, Macromolecules 32 (6) (1999) 1785–1796.
[35] P.I. Vincent, A correlation between critical tensile strength and polymer cross-sectional area, Polymer 13 (12) (1972) 558–560.
[36] M.D. Goodner, C.N. Bowman, Development of a comprehensive free radical photopolymerization model incorporating heat and mass transfer effects in thick films, Chem. Eng. Sci. 57 (5) (2002) 887–900.
[37] K.N. Long, et al., Photomechanics of light-activated polymers, J. Mech. Phys. Solids 57 (7) (2009) 1103–1121.
[38] T.C. Merkel, et al., Gas sorption, diffusion, and permeation in poly(dimethylsiloxane), J. Polym. Sci. Part B 38 (3) (2000) 415–434.
[39] H.Q. Lin, B.D. Freeman, Gas permeation and diffusion in cross-linked poly(ethylene glycol diacrylate), Macromolecules 39 (10) (2006) 3568–3580.
[40] E. Andrzejewska, Photopolymerization kinetics of multifunctional monomers, Prog. Polym. Sci. 26 (4) (2001) 605–665.